Detailed chemical compositions of planet-hosting stars – I. Exploration of possible planet signatures

F. Liu [ORCID],[1][*] D. Yong,[2] M. Asplund,[2] H. S. Wang,[3] L. Spina,[4,5] L. Acuña,[6] J. Meléndez[7] and I. Ramírez[8]

[1]*Centre for Astrophysics and Supercomputing, Swinburne University of Technology, Melbourne, VIC 3122, Australia*
[2]*Research School of Astronomy and Astrophysics, Australian National University, Canberra, ACT 2611, Australia*
[3]*Institute for Particle Physics and Astrophysics, ETH Zürich, Wolfgang-Pauli-Strasse 27, CH-8093 Zürich, Switzerland*
[4]*Monash Centre for Astrophysics, School of Physics and Astronomy, Monash University, Melbourne, VIC 3800, Australia*
[5]*ARC Centre of Excellence for All Sky Astrophysics in Three Dimensions (ASTRO-3D), Australia*
[6]*Laboratoire d'Astrophysique de Marseille, Aix-Marseille University, F-13388 Marseille cedex 13, France*
[7]*Departamento de Astronomia do IAG/USP, Universidade de Sao Paulo, Rua do Matao 1226, Sao Paulo 05508-900, Brazil*
[8]*Tacoma Community College, 6501 South 19th Street, Tacoma, WA 98466, USA*

ABSTRACT

We present a line-by-line differential analysis of a sample of 16 planet-hosting stars and 68 comparison stars using high-resolution, high signal-to-noise ratio spectra gathered using Keck. We obtained accurate stellar parameters and high-precision relative chemical abundances with average uncertainties in $T_{\rm eff}$, log g, [Fe/H], and [X/H] of 15 K, 0.034 cm s^{-2}, 0.012 dex, and 0.025 dex, respectively. For each planet host, we identify a set of comparison stars and examine the abundance differences (corrected for Galactic chemical evolution effect) as a function of the dust condensation temperature, $T_{\rm cond}$, of the individual elements. While we confirm that the Sun exhibits a negative trend between abundance and $T_{\rm cond}$, we also confirm that the remaining planet hosts exhibit a variety of abundance–$T_{\rm cond}$ trends with no clear dependence upon age, metallicity, or $T_{\rm eff}$. The diversity in the chemical compositions of planet-hosting stars relative to their comparison stars could reflect the range of possible planet-induced effects present in these planet hosts, from the sequestration of rocky material (refractory poor) to the possible ingestion of planets (refractory rich). Other possible explanations include differences in the time-scale, efficiency and degree of planet formation, or inhomogeneous chemical evolution. Although we do not find an unambiguous chemical signature of planet formation among our sample, the high-precision chemical abundances of the host stars are essential for constraining the composition and structure of their exoplanets.

Key words: planets and satellites: terrestrial planets – stars: abundances – stars: atmospheres.

1 INTRODUCTION

The detection and characterization of exoplanets remains a major focus in modern astronomy. Since the discovery of the first exoplanet around a solar-type star (Mayor & Queloz 1995), thousands of confirmed exoplanets have been discovered through a raft of methods, the most successful being radial velocity variations and transit photometry. Arguably the greatest surprise has been the enormous diversity in the properties of exoplanets (Winn & Fabrycky 2015).

A star and its planets are believed to arise from the same molecular cloud. The properties of the host star likely influence the protoplanetary disc in which the planets form. Vice versa, accretion of materials from the protoplanetary disc on to the host star may also implant disc/planet signatures into the host stars. Correlations between the properties of planets and the characteristics of their host stars may therefore provide crucial insight into the planet formation process.

Soon after the first exoplanets were discovered, it was recognized that the frequency of hot Jupiters increased rapidly with the overall metallicity of the host star (e.g. Gonzalez 1997; Fischer & Valenti 2005) with iron being the canonical measure of stellar metallicity. The metallicity dependence is typically interpreted as support for the core accretion model of giant planet formation (Pollack et al. 1996), while in the rival disc instability model (Boss 1997) no such correlation is expected.

In their pioneering study, Meléndez et al. (2009, hereafter M09) applied a strictly differential line-by-line analysis of high-quality

[*] E-mail: fanliu@swin.edu.au

spectra ($R = 65\,000$, signal-to-noise ratio S/N $\sim$ 450) of a sample of solar twins (stars with essentially identical parameters to the Sun). This approach enabled relative chemical abundance measurements to be obtained with unprecedented precision at the $\sim$0.01 dex level (see Nissen & Gustafsson 2018 for an overall review of the method and Bedell et al. 2014 for a discussion of systematic uncertainties). M09 found that the Sun was chemically peculiar when compared to the majority of solar twins (about 15 per cent of solar twins share the solar chemical composition). A striking correlation was found when plotting the abundance differences (Sun with respect to the average of the solar twins) as a function of the dust condensation temperature ($T_{\rm cond}$) of the individual elements.

M09 suggested that this correlation may represent the chemical signature of terrestrial planet formation. While these results have been confirmed and extended to additional planet hosts by some investigators (e.g. Ramírez, Meléndez & Asplund 2009; Gonzalez, Carlson & Tobin 2010; Ramírez et al. 2010; Schuler et al. 2011; Liu et al. 2016), the interpretation remains contentious with other groups finding conflicting results (e.g. González Hernández et al. 2010, 2013; Adibekyan et al. 2014). Nissen (2015, 2016) suggested that the dependence of chemical abundance ratios, [X/Fe], on stellar age complicates the planet signature hypothesis of M09. More recently, it has been proposed that the M09 signature possibly arises from the formation of Jupiter analogues (i.e. giant planets at large separations), rather than being a signature of rocky planets (Booth & Owen 2020).

In addition, post-formation accretion of planets on to the host star can also alter its stellar surface abundances. If the host star is polluted after its birth by refractory-rich planetary material, the convective envelope of the star may be enhanced in high-$T_{\rm cond}$ elements (e.g. Pinsonneault, DePoy & Coffee 2001). Such a process can produce the $T_{\rm cond}$-dependent trend showing enrichment of chemical abundances for refractory elements in the planet-host star. This has been reported in a few spectroscopic studies of wide binaries (e.g. Liu et al. 2018; Oh et al. 2018; Ramírez et al. 2019; Nagar et al. 2020). Recent studies also found evidences in open clusters (Spina et al. 2015, 2018a). For example, in Spina et al. (2015) they found that the anomalous star is more metal rich than the average metallicity of the cluster stars, meaning that such a star has been polluted and not vice versa.

Other hypothesis that has been explored regarding the trend with condensation temperature found by M09 is dust cleansing by massive stars from the same cluster where the Sun was born (Gustafsson 2018a), or even by radiation of the proto-Sun itself (Gustafsson 2018b).

To further explore any potential stellar chemical signature of planet formation, we present a differential chemical abundance analysis of 16 planet-hosting stars. The sample selection, observations, data reduction, and analysis are described in Section 2. The results and discussion are in Sections 3 and 4, respectively. We summarize and conclude in Section 5.

2 SAMPLE SELECTION, OBSERVATIONS, DATA REDUCTION, AND ANALYSIS

Potential planet hosts were identified by querying the exoplanets.org website (Han et al. 2014). Planets with $M < 0.1\,M_{\rm Jupiter}$ orbiting sufficiently bright stars ($V < 12.5$) with effective temperatures well suited for a differential abundance analysis ($5400 < T_{\rm eff} < 6400$ K) were selected.

A set of comparison stars (objects not known at that time to host planets) was identified from various literature sources, including Ramírez & Meléndez (2005), Bensby, Feltzing & Oey (2014), and Reddy et al. (2003). The primary criterion was to select bright stars with similar $T_{\rm eff}$, $\log g$, and [Fe/H] to the planet hosts. Since the goal of this study was to identify whether or not planet-hosting stars are chemically peculiar, it is important to minimize the abundance errors by ensuring that the stellar parameters of the planet hosts and comparison stars are as similar as possible. This selection process, however, suffered from the heterogeneous nature of the sample (i.e. there are systematic offsets in the stellar parameters between the various publications). To mitigate this potential problem, *Gaia* data (Gaia Collaboration et al. 2016, 2018) were also employed to ensure that the comparison stars occupied similar locations in the $M_{\rm G}$ versus BP $-$ RP colour–magnitude diagram.

A total of 16 planet hosts and 68 comparison stars were observed using the High Resolution Echelle Spectrometer (HIRES; Vogt et al. 1994) on the 10-m Keck I telescope on 2016 May 18, 2016 August 13, and 2018 July 4. Following Liu et al. (2014), we used the B2 slit with a width of 0.574 arcsec that provided a spectral resolution of $R = 67\,000$. For all objects, we aimed to achieve S/N = 300 pixel^{-1} near 6000 Å. A higher S/N spectrum was obtained for the asteroid Iris that we use hereafter as a solar spectrum. The wavelength coverage is nearly complete from 3800 to 8000 Å. The MAuna Kea Echelle Extraction (MAKEE) data reduction package at the Keck Observatory was used to reduce the raw HIRES spectra. Individual spectra were co-added and normalized using IRAF[1]. Example of a portion of the spectra is shown in Fig. 1.

Equivalent widths were measured in each star for a set of lines taken from Liu et al. (2014). The line list and equivalent width measurements are presented in Table A1. Following M09 and Meléndez et al. (2012), the effective temperature ($T_{\rm eff}$) was obtained by forcing excitation balance for Fe I lines based on a line-by-line differential analysis with respect to the Sun. The surface gravity ($\log g$) was set when ionization balance between Fe I and Fe II was achieved. The microturbulent velocity ($\xi_{\rm t}$) was obtained when there was no trend between the abundance from Fe I lines and the reduced equivalent width. Following Ramírez et al. (2014), we used the QOYLLUR-QUIPU (Q^2)[2] code to perform the differential abundance analysis and to compute the uncertainties. The adopted parameters for the Sun are fixed as $T_{\rm eff} = 5772$ K, $\log g = 4.44$ cm s^{-2}, $\xi_{\rm t} = 1.00$ km s^{-1}, and [Fe/H] = 0.00 dex. Stellar ages were also computed using Q^2 by fitting Yonsei–Yale isochrones (Demarque et al. 2004), based on the *Gaia* Data Release 2 (DR2) distances as presented in Bailer-Jones et al. (2018), $T_{\rm eff}$ and the metallicity, [Fe/H], from this study. As noted in Lin et al. (2020), multiple factors can lead to high and unrealistic ages from isochrone fitting. We note that the oldest stars in our sample have ages of 15.1 Gyr, but that none of the objects older than 10 Gyr are used in the abundance comparisons with the planet hosts.

The uncertainties for the stellar parameters $T_{\rm eff}$, $\log g$, and $\xi_{\rm t}$ were computed using the approach in Epstein et al. (2010) and Bensby et al. (2014). For [Fe/H], the uncertainty was obtained by propagating the errors for the stellar parameters noted above then adding them in quadrature (which conservatively assumes that they are uncorrelated) and including the standard error of the mean from

---

[1] IRAF is distributed by the National Optical Astronomy Observatories, which are operated by the Association of Universities for Research in Astronomy, Inc., under cooperative agreement with the National Science Foundation.

[2] QOYLLUR-QUIPU or Q^2 is a PYTHON package available online at https://github.com/astroChasqui/q2.
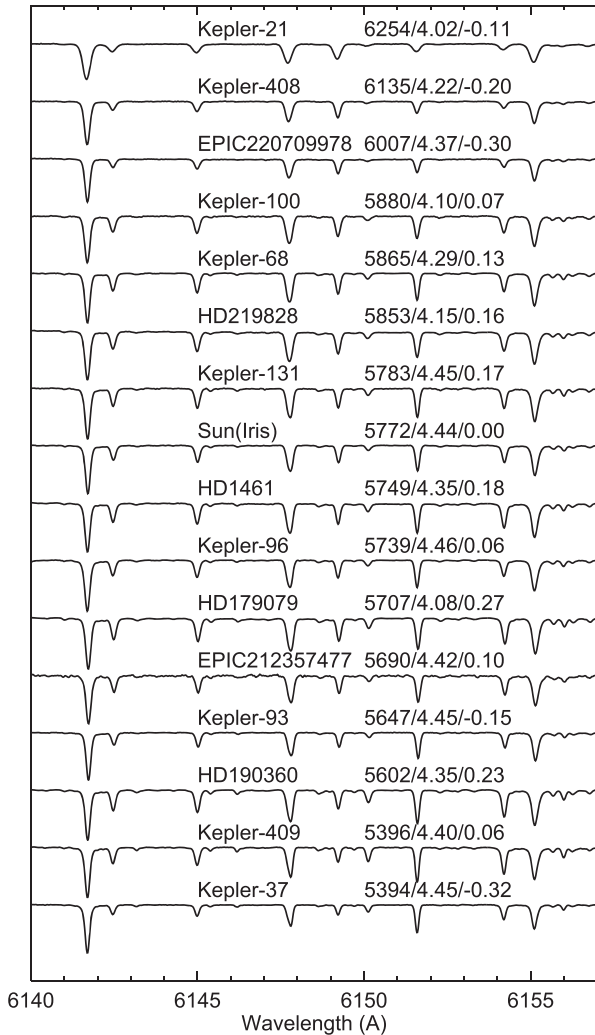
Figure 1. A portion of the spectra for the 16 planet hosts. The stellar parameters (T_{eff}, $\log g$, and [Fe/H]) are included in the figure and the stars are ordered by T_{eff} from hot (top) to cool (bottom).

line-to-line scatter. For the uncertainties in abundance ratios [X/H], we adopt the same approach as for [Fe/H].

The differential stellar parameters and their uncertainties are presented in Table 1. The abundances and their uncertainties are given in Table 2. With the exception of O, all abundances were derived under the approximation of local thermodynamic equilibrium (LTE). For the O abundances that were derived from the 777 nm triplets, non-LTE corrections from Ramírez, Allende Prieto & Lambert (2007) were applied.

In Fig. 2, we show the locations of the stars in the T_{eff} versus $\log g$ plane with the data colour coded by the metallicity. All stars lie on the main sequence or main-sequence turn-off and have metallicities in the range $-0.32 \leq$ [Fe/H] $\leq +0.27$. We note that there are ~5–12 comparison stars locate around each planet host. The stellar parameters have small uncertainties due to the high-quality spectra and differential nature of the analysis. The average uncertainties for T_{eff}, $\log g$, ξ_{t}, and [Fe/H] are 15 K, 0.034 cm s^{-2}, 0.035 km s^{-1} and 0.012 dex, respectively. We note that the average uncertainties in stellar parameters for the planet hosts are essentially identical to the corresponding values for the comparison stars.

The distribution of the abundance uncertainties for each element, σ[X/H], is presented in Fig. 3. The first point to note is that the average abundance uncertainties are small, in the range 0.010 dex (for Si) to 0.042 dex (for C). Such high-precision relative chemical abundance measurements can be attributed to the small uncertainties in stellar parameters that in turn are due to the differential analysis of high-quality spectra. The second point to note is that, modulo small number statistics, the average abundance error for a given element is the same for the planet-host population and for the comparison stars.

3 RESULTS

We now examine the trends between abundance ratios [X/Fe] versus [Fe/H] (left-hand panels) in Figs 4–6. In all panels, we present the linear fit to the comparison stars, i.e. we exclude from the fit the planet hosts, thick disc objects, stars with ages ≥ 10 Gyr, and HD 138004 with [Y/Fe] $= +0.92$ that we hereafter refer to as a s-process-rich object.

In Table 3, we present the coefficients a and b for the fit to the relation [X/Fe] $= a \times$ [Fe/H] $+ b$. The abundance trends [X/Fe] versus [Fe/H] are well defined, and the dispersion about the linear fit is small, ranging from 0.016 dex (for Ca) to 0.075 dex (for C) with an average value of 0.046 dex.

Overall, our abundance measurements are of high precision due to the high-quality spectra and differential abundance analysis. We note, however, that the analyses by Spina et al. (2018b) and Bedell et al. (2018) achieved even better abundance precision most likely because their sample spanned a considerably smaller range in stellar parameters $\Delta T_{\mathrm{eff}} = 283$ K, $\Delta \log g = 0.445$ cm s^{-2}, and Δ[Fe/H] $=$ 0.285 dex, while the corresponding values for this study are 1088 K, 0.665 cm s^{-2}, and 0.882 dex, respectively.

Examination of the [α/Fe] versus [Fe/H] in Fig. 6 indicates that there are four stars that lie above the general trend. We refer to those objects as thick disc stars as they exhibit abundance trends in accordance with that stellar population (e.g. Venn et al. 2004), and we note that their ages are consistent with an older population: HD 11505 (11.7 Gyr), HIP 14241 (15.1 Gyr), HD 136274 (14.2 Gyr), and HD 187923 (9.3 Gyr). Additionally, there are three stars with ages greater than 10 Gyr. While these objects exhibit thin-disc-like [α/Fe] ratios, we highlight these stars in various figures and refer to them as 'old disc' objects: HD 7438 (10.3 Gyr), HD 164922 (11.6 Gyr), and HD 172310 (11.2 Gyr).

As recognized by Nissen (2015), Liu et al. (2016), Spina, Meléndez & Ramírez (2016), Bedell et al. (2018), and others, it is important to consider Galactic chemical evolution (GCE) effects when comparing stars with different ages even if they have similar T_{eff} and [Fe/H]. To that end, we present the abundance trends [X/Fe] versus age (right-hand panels) in Figs 4–6. As before, we include the linear fit to the comparison stars excluding the planet hosts, thick disc, old disc, and s-process-rich objects. Table 4 includes the coefficients a and b for the relation [X/Fe] $= a \times$ age $+ b$. We confirm previous results that the [Y/Al] ratio exhibits a steep dependence upon stellar age, -0.040 dex Gyr^{-1}. For comparison, Nissen (2016) and Spina et al. (2018b) find slopes of -0.0427 and -0.051 dex Gyr^{-1}, respectively. Based on the coefficients presented in Table 4, the [Y/Zn] ratio would also exhibit a steep dependence on age, -0.034 dex Gyr^{-1} (see also Jofré, Jackson & Tucci Maia 2020 for other potential chemical clocks).

Using these fits, we can obtain GCE-corrected abundance ratios: [X/Fe]$_{\mathrm{GCE\ corrected}} =$ [X/Fe]$_{\mathrm{raw}} - (a \times$ age $+ b)$, where a and b are from Table 4. We derived GCE-corrected abundances for all

Table 1. Stellar parameters and ages for the program stars.

| Name	RA (J2000)	Dec. (J2000)	T_{eff} (K)	log g (cm s^{-2})	ξ_t (km s^{-1})	[Fe/H] (dex)	Age (Gyr)	Age[a] (Gyr)	Age[b] (Gyr)
				Planet hosts					
Sun (Iris)	...	...	5774	4.440	1.00	0.000	4.6		
HD 1461	00 18 42.30	−08 03 13.03	5749 ± 10	4.345 ± 0.029	1.05 ± 0.03	0.180 ± 0.010	5.3	4.8	5.9
EPIC 220709978	01 05 51.00	+11 45 13.38	6007 ± 19	4.372 ± 0.049	1.32 ± 0.05	− 0.296 ± 0.014	6.0	5.3	6.7
EPIC 212357477	13 28 03.88	−15 56 16.70	5690 ± 16	4.420 ± 0.049	1.01 ± 0.05	0.100 ± 0.017	3.0	1.6	4.5
Kepler-37	18 56 14.22	+44 31 06.14	5394 ± 8	4.452 ± 0.026	0.77 ± 0.03	− 0.322 ± 0.008	7.9	5.8	10.1
Kepler-408	18 59 08.69	+48 25 23.74	6135 ± 19	4.218 ± 0.045	1.45 ± 0.04	− 0.201 ± 0.014	4.2	3.8	4.8
Kepler-21	19 09 26.87	+38 42 50.89	6254 ± 25	4.015 ± 0.044	1.74 ± 0.06	− 0.110 ± 0.016	3.8	3.2	4.1
HD 179079	19 11 09.68	−02 38 19.57	5707 ± 22	4.083 ± 0.042	1.17 ± 0.04	0.272 ± 0.018	6.5	6.1	6.8
Kepler-131	19 14 07.41	+40 56 32.54	5783 ± 10	4.445 ± 0.026	1.03 ± 0.03	0.166 ± 0.011	1.4	0.6	2.6
Kepler-68	19 24 07.75	+49 02 24.76	5865 ± 6	4.293 ± 0.016	1.13 ± 0.01	0.126 ± 0.005	5.3	4.9	5.9
Kepler-93	19 25 40.35	+38 40 20.32	5647 ± 6	4.445 ± 0.020	0.92 ± 0.02	− 0.146 ± 0.006	6.9	5.6	7.8
Kepler-100	19 25 32.67	+41 59 24.50	5880 ± 18	4.103 ± 0.035	1.28 ± 0.03	0.070 ± 0.014	6.6	6.2	6.9
Kepler-409	19 34 43.00	+46 51 09.84	5396 ± 12	4.400 ± 0.035	0.82 ± 0.04	0.059 ± 0.012	8.9	6.9	10.2
Kepler-96	19 48 16.75	+40 31 30.73	5739 ± 4	4.460 ± 0.014	0.95 ± 0.01	0.059 ± 0.004	2.6	1.2	3.2
HD 190360	20 03 38.21	+29 53 40.34	5602 ± 17	4.350 ± 0.042	1.04 ± 0.05	0.228 ± 0.017	7.6	6.7	8.9
HD 219828	23 18 46.72	+18 38 44.70	5853 ± 17	4.147 ± 0.034	1.27 ± 0.03	0.160 ± 0.013	6.0	5.4	6.3
				Comparison stars					
HD 166	00 06 37.23	+29 01 14.65	5535 ± 13	4.500 ± 0.031	1.18 ± 0.04	0.099 ± 0.013	1.7	0.6	3.4
HD 4813	00 50 07.34	−10 38 43.14	6217 ± 19	4.353 ± 0.055	1.34 ± 0.05	− 0.095 ± 0.013	2.7	2.2	3.1
HD 4915	00 51 11.11	−05 02 23.24	5658 ± 8	4.475 ± 0.026	0.94 ± 0.02	− 0.192 ± 0.007	5.0	3.5	6.3
HD 6250	01 04 16.35	+54 12 14.31	6216 ± 22	4.030 ± 0.039	1.72 ± 0.05	− 0.150 ± 0.015	4.0	3.3	4.3
HD 7438	01 14 22.55	−07 54 35.04	5247 ± 13	4.462 ± 0.037	0.74 ± 0.05	− 0.278 ± 0.011	10.3	7.4	12.7

Note. This table is published in its entirety in the electronic edition of the paper. A portion is shown here for guidance regarding its content. [a]Lower limit. [b]Upper limit.

Table 2. Relative abundances for the program stars.

Name	[C/H]	σ[C/H]	[O/H]	σ[O/H]	[Na/H]	σ[Na/H]	[Mg/H]	σ[Mg/H]	[Al/H]	σ[Al/H]	...
					Planet hosts						
Sun (Iris)	0.000	...	0.000	...	0.000	...	0.000	...	0.000	...	...
HD 1461	0.215	0.033	0.126	0.018	0.291	0.030	0.173	0.009	0.260	0.029	...
EPIC 220709978	− 0.191	0.122	− 0.254	0.021	− 0.261	0.028	− 0.259	0.014	− 0.316	0.038	...
EPIC 212357477	0.167	0.066	0.092	0.027	0.091	0.027	0.059	0.016	0.132	0.010	...
Kepler-37	− 0.284	0.030	− 0.201	0.011	− 0.340	0.018	− 0.199	0.009	− 0.150	0.102	...
Kepler-408	− 0.178	0.028	− 0.205	0.024	− 0.232	0.039	− 0.150	0.013	− 0.220	0.022	...
Kepler-21	− 0.091	0.043	− 0.069	0.028	− 0.065	0.045	− 0.111	0.015	− 0.237	0.009	...
HD 179079	0.381	0.046	0.205	0.037	0.382	0.023	0.272	0.017	0.378	0.022	...
Kepler-131	0.093	0.070	0.072	0.015	0.125	0.023	0.129	0.010	0.200	0.014	...
Kepler-68	0.053	0.015	0.063	0.010	0.139	0.016	0.130	0.005	0.313	0.126	...
Kepler-93	− 0.163	0.040	− 0.097	0.010	− 0.161	0.017	− 0.095	0.006	− 0.039	0.038	...
Kepler-100	0.171	0.020	0.078	0.026	0.151	0.019	0.091	0.013	0.152	0.028	...
Kepler-409	0.085	0.015	...	...	0.094	0.048	0.096	0.014	0.215	0.050	...
Kepler-96	− 0.045	0.021	− 0.007	0.007	− 0.046	0.007	0.017	0.004	0.010	0.028	...
HD 190360	0.386	0.034	0.240	0.021	0.270	0.037	0.346	0.018	0.455	0.071	...
HD 219828	0.172	0.047	0.136	0.025	0.271	0.022	0.144	0.014	0.260	0.025	...
					Comparison stars						
HD 166	0.081	0.043	0.070	0.017	0.069	0.027	0.064	0.015	0.103	0.017	...
HD 4813	− 0.055	0.096	− 0.089	0.024	− 0.129	0.032	− 0.120	0.013	− 0.230	0.032	...
HD 4915	− 0.005	0.008	− 0.140	0.010	− 0.234	0.015	− 0.150	0.007	− 0.175	0.035	...
HD 6250	− 0.102	0.026	− 0.129	0.031	− 0.114	0.043	− 0.145	0.013	− 0.209	0.021	...
HD 7438	− 0.087	0.013	− 0.167	0.017	− 0.320	0.027	− 0.189	0.014	− 0.207	0.016	...

Note. This table is published in its entirety in the electronic edition of the paper. A portion is shown here for guidance regarding its content.

objects. In the following discussion and analysis, we adopt these GCE-corrected [X/Fe] abundance ratios.

In order to explore the chemical peculiarity of each planet-hosting star, we first need to identify the best set of comparison stars by selecting its nearest neighbours in stellar parameter space using the following approach. Taking the planet host Kepler-68 as an example, as shown in Fig. 7, we plot [Fe/H] versus T_{eff}. We define an ellipse with a major axis of 100 K in T_{eff} and a minor axis of 0.1 dex in [Fe/H]. Keeping the major to minor axial ratio fixed, we then increase or decrease the ellipse until there are 12 comparison stars within that ellipse (as before, we exclude thick disc, old disc, and s-process-rich objects when selecting the nearest comparison stars).
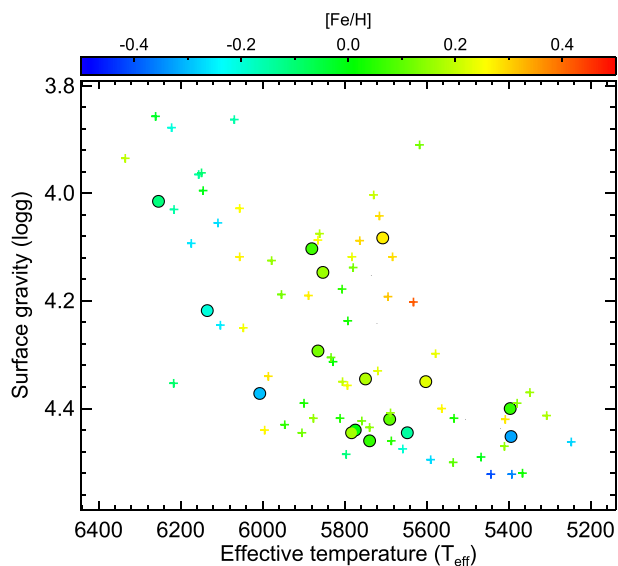
Figure 2. Effective temperature ($T_{\rm eff}$) versus surface gravity (log g). Planet hosts are shown as circles while the comparison stars are crosses; all objects are coloured by metallicity. There are sufficient comparison stars locate around each planet host.

In the case of Kepler-68 (Fig. 7), the maximum difference in $T_{\rm eff}$ and [Fe/H] between the planet host and the comparison stars was 107 K and 0.107 dex, respectively. When selecting these nearest comparison stars, we arbitrarily imposed a maximum distance of 300 K in $T_{\rm eff}$ and 0.3 dex in [Fe/H]. In some instances this resulted in fewer than 12 comparison stars for a given planet host; Kepler-21, Kepler-37, Kepler-408, and EPIC 220709978 had 11, 5, 11, and 9 comparison stars, respectively. The rationale in imposing a maximum distance in $T_{\rm eff}$ and [Fe/H] for the comparison stars was to ensure that the stellar parameters of the planet hosts and comparison stars were as similar as possible and thereby obtain precise and reliable abundance differences.

We note that our sample spans over a range of [Fe/H], which might induce subtle scatter for our GCE corrections since the slopes of [X/Fe] versus ages can change with [Fe/H]. However, our sample, i.e. each set of a planet host and its comparison stars, is not large enough to be separated into different [Fe/H] bins to minimize such effects. In addition, the age–[Fe/H] relation is basically flat with considerable scatter (see e.g. Bensby et al. 2014). For future analysis of a larger sample, it would be useful for GCE corrections to include both age and [Fe/H].

In Fig. 8, we plot the abundance differences (GCE corrected) between Kepler-68 (upper), Kepler-93 (middle), and Kepler-100 (lower) and the average of the 12 nearest comparison stars (Δ[X/Fe]$_{\rm GCE\ corrected}$) versus the condensation temperature of each element, $T_{\rm cond}$, taken from Lodders (2003). The standard errors of the average abundances of comparison stars were taken into account by adding in quadrature to the errors of abundances of the corresponding planet host as the total uncertainties in the abundance differences between each planet host and the average of its comparison stars. These three representative objects exhibit a positive, zero, and negative abundance trend with $T_{\rm cond}$. In that figure, we highlight four quantities of interest. (1) The slope (and uncertainty and dispersion about the linear fit) for all elements. (2) Same as (1) but for the volatile elements with $T_{\rm cond} < 1200$ K. (3) Same as (1) but for the refractory elements with $T_{\rm cond} > 1200$ K. (4) The difference between the average Δ[X/Fe]$_{\rm GCE\ corrected}$ for the
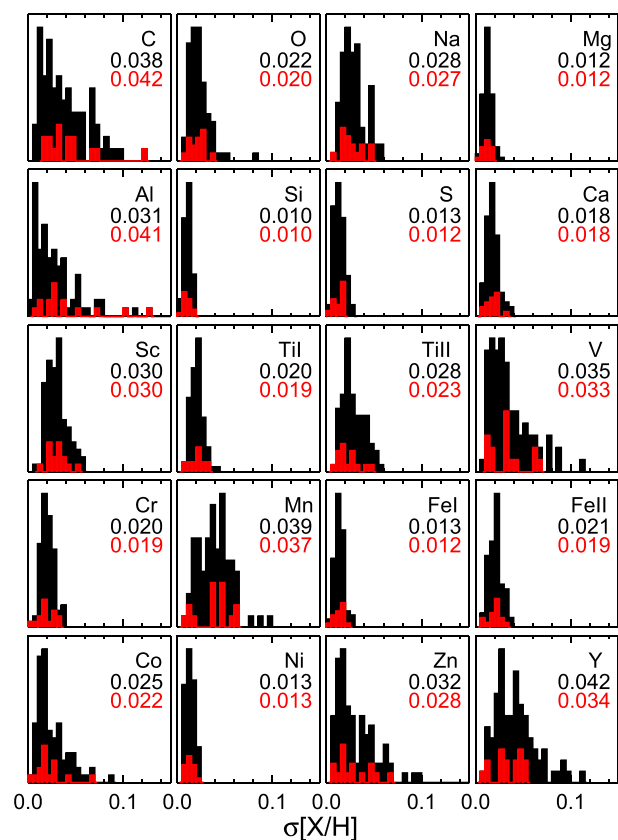

Figure 3. The error distribution for each element, [X/H], for all stars (black histogram) and planet hosts (red histogram). The average error is written in each panel.

volatile (v) and refractory (r) elements, [v/r]. We repeated the same exercise for all 16 planet hosts and summarize those analyses in Table 5 and in Fig. 9 where the data are colour coded by the effective temperature.

We also considered only the 10 nearest neighbours (rather than 12) and our conclusions are unchanged. Similarly, our conclusions are unchanged when using the raw [X/Fe] ratios. Finally, we chose not to use the high-fidelity GCE corrections from Spina et al. (2018b) and Bedell et al. (2018) since they were derived from their analysis of a different sample. Had we applied their GCE corrections, however, our conclusions would remain the same. Therefore, we are confident that our results are reliable.

An independent analysis of a subset of these stars was conducted by Acuña (2019). There is an excellent agreement for the stellar parameters and abundances between the two analyses. We now briefly discuss the comparison between our results and select literature values (we do not undertake an exhaustive search of the literature for all program stars).

There are four planet hosts in common between this study and Schuler et al. (2015): Kepler-21, Kepler-37, Kepler-68, and Kepler-100. Their analysis was based on high-resolution, high S/N spectra. Our stellar parameters are in excellent agreement with Schuler et al. (2015) with average differences (this study − Schuler et al.) in $T_{\rm eff}$, log g, and [Fe/H] of 10 ± 23 K, -0.01 ± 0.06 cm s^{-2}, and -0.01 ± 0.01 dex, respectively. For the elements common to both studies, we find an average difference (this study − Schuler et al.) in abundance ratios [X/H] of 0.00 ± 0.02, 0.02 ± 0.01, 0.00 ± 0.01,
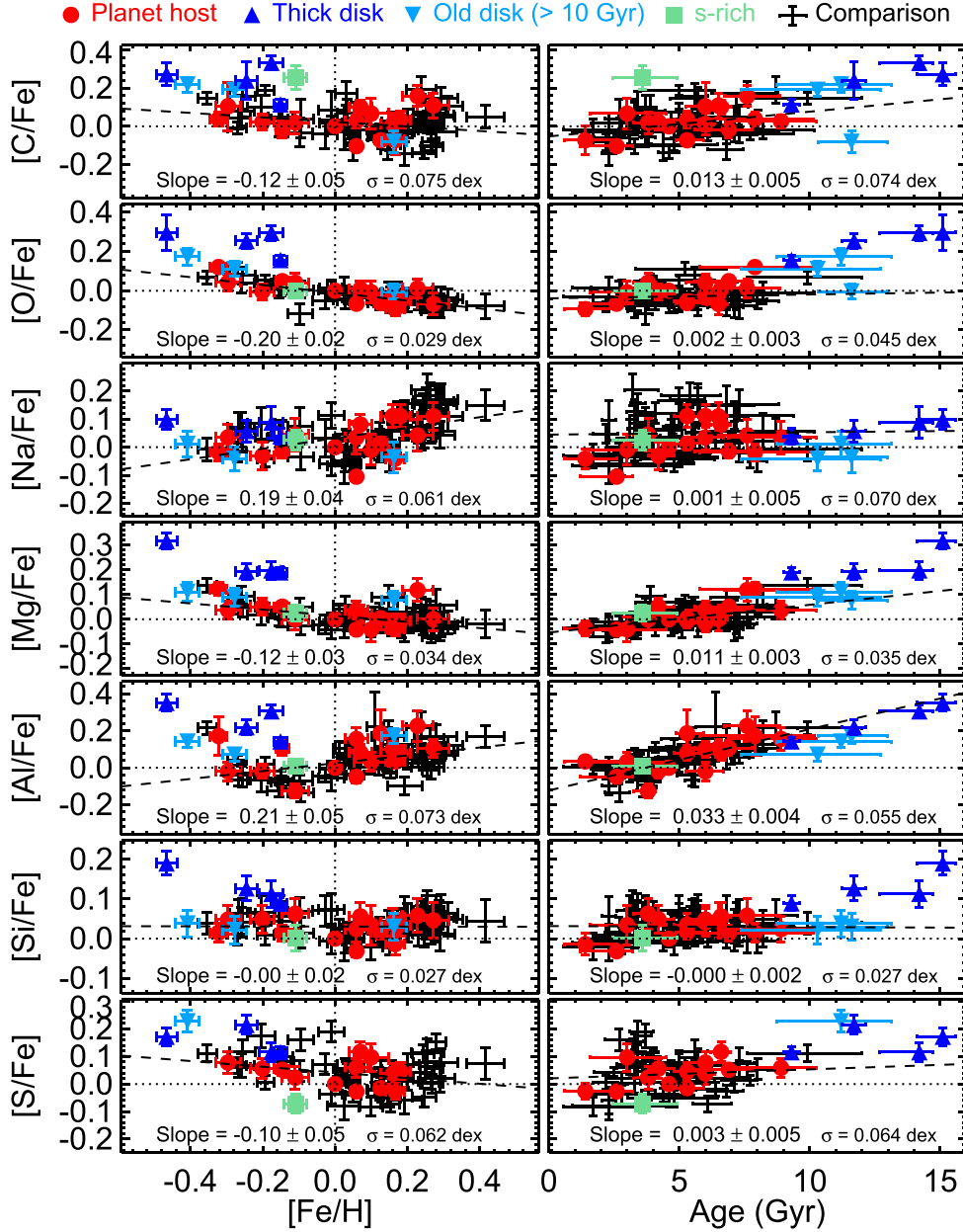
Figure 4. [X/Fe] versus [Fe/H] (left-hand panels) and ages (right-hand panels) for the first seven elements. The best-fitting slope to the comparison stars is overplotted. The slope and dispersion about the fit are written in each panel.

and 0.00 ± 0.01 for Kepler-21, Kepler-37, Kepler-68, and Kepler-100, respectively.

Petigura et al. (2017) determined stellar parameters for 1305 Kepler objects including nine in common with this study. Our stellar parameters are in good agreement with theirs with average differences (this study − Petigura et al.) in $T_{\rm eff}$, log g, and [Fe/H] of 29 ± 11 K, -0.022 ± 0.023 cm s^{-2}, and -0.046 ± 0.007 dex, respectively.

Brewer et al. (2016) measured stellar parameters and chemical abundances for 1617 stars including nine Kepler objects in this study. The agreement in stellar parameters is very good with average differences (this study − Brewer et al.) in $T_{\rm eff}$, log g, and [Fe/H] of 34 ± 11 K, -0.027 ± 0.022 cm s^{-2}, and -0.008 ± 0.014 dex, respectively. For the elements common to both studies, we find an average difference in abundance ratios [X/H] of 0.006 ± 0.006 dex

for the nine common stars. Overall, our results appear to be in very good agreement with literature values.

4 DISCUSSION

As noted in the Introduction, M09 found a striking negative trend between the abundance differences (Sun minus the average for a sample of solar twins) versus $T_{\rm cond}$. In Fig. 9, the Sun is located at [Fe/H] $= 0.00$ and has a slope for all elements of $-0.32 \pm 0.12 \times 10^{-4}$ dex K^{-1}. Among the other 15 planet hosts, nine have negative slopes for the abundance differences versus $T_{\rm cond}$ while the remaining six have positive slopes. There is no significant dependence ($>3\sigma$) of these abundance trends as a function of ages or [Fe/H]. Similarly, there is no obvious dependence of these abundance trends with $T_{\rm eff}$.
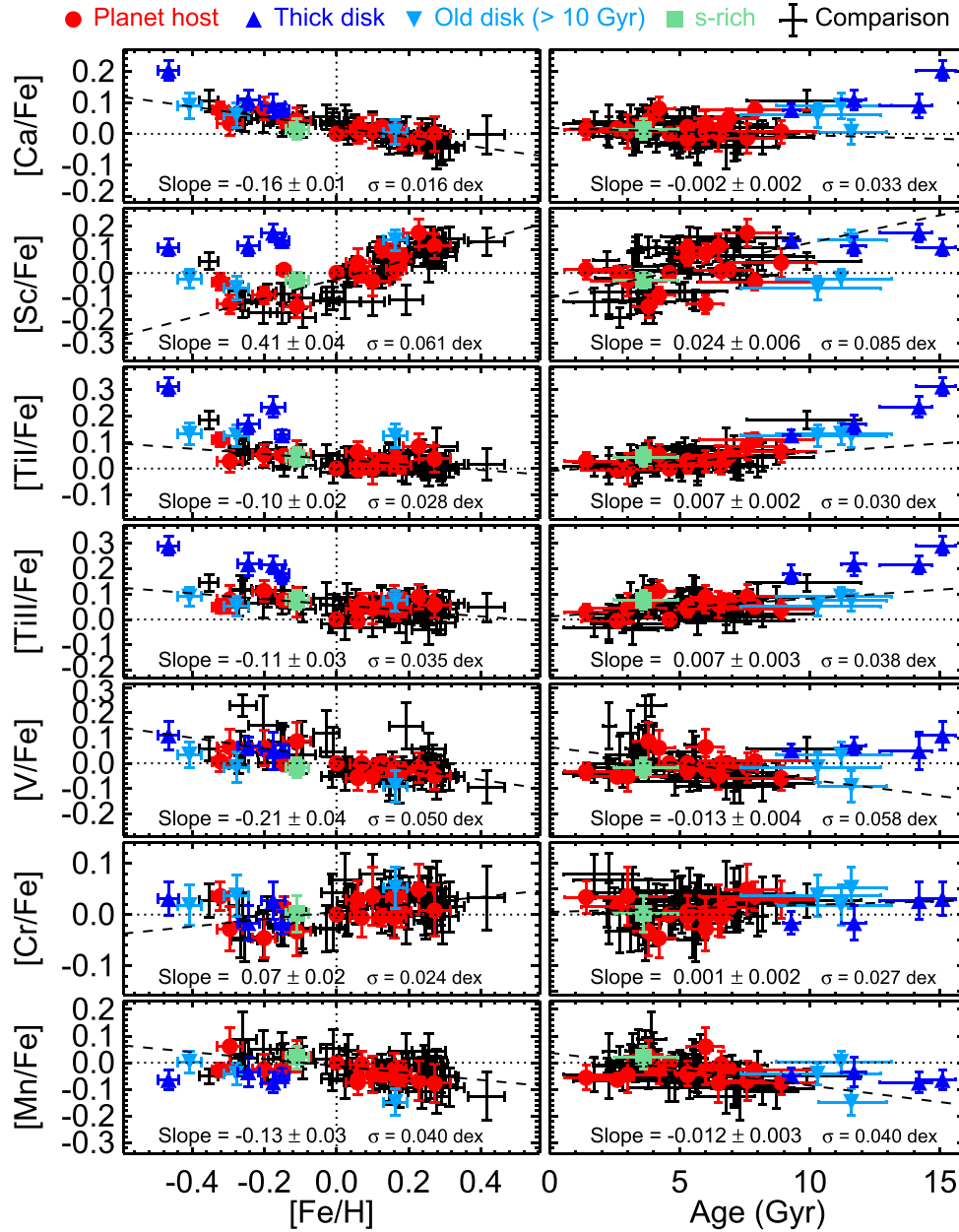
Figure 5. Same as Fig. 4, but for the next seven elements.

The strongest trends are for slope of the ratio of volatile to refractory elements [v/r] versus ages, but they are only significant at the ∼2σ level. For the Sun, the ratio of volatile to refractory elements is [v/r] = +0.021 dex (bottom panel in Fig. 9). Among the other 15 planet hosts, nine have positive values of [v/r] while the remaining six have negative values.

Recall that in Fig. 9, GCE corrections have been applied. Furthermore, we have also examined similar versions of this plot using the raw [X/Fe] ratios and when applying GCE corrections from Spina et al. (2018b) and Bedell et al. (2018). In all cases, our conclusions would not change and there are no obvious correlations between abundance trends and ages or [Fe/H].

In the M09 hypothesis, the proto-Sun is surrounded by a proto-planetary disc. In that protoplanetary disc, the refractory elements are preferentially locked-up in planetesimals and subsequently in the terrestrial planets. As a consequence, most of the remaining materials, which are more volatile, in the protosolar disc are eventually accreted back on to the Sun. The abundance differences between the Sun and the comparison stars could be produced if those comparison stars did not form planets (for whatever reason). Alternatively, planet formation may have proceeded more efficiently in the Solar system than for typical stars.

If we assume that the M09 hypothesis is correct, i.e. terrestrial planet formation can induce a subtle chemical abundance signature, then roughly half of our sample would appear to exhibit a similar phenomenon (i.e. negative abundance trends versus T_{cond}) albeit to different degrees. Any scenarios supporting this hypothesis would then need to account for the diversity in abundance differences as a function of T_{cond} amongst the different planet-hosting stars.

For the other half of the sample, however, the abundance trends versus T_{cond} exhibit the opposite sign. In the M09 scenario, this could indicate that the comparison stars formed more planets and/or more
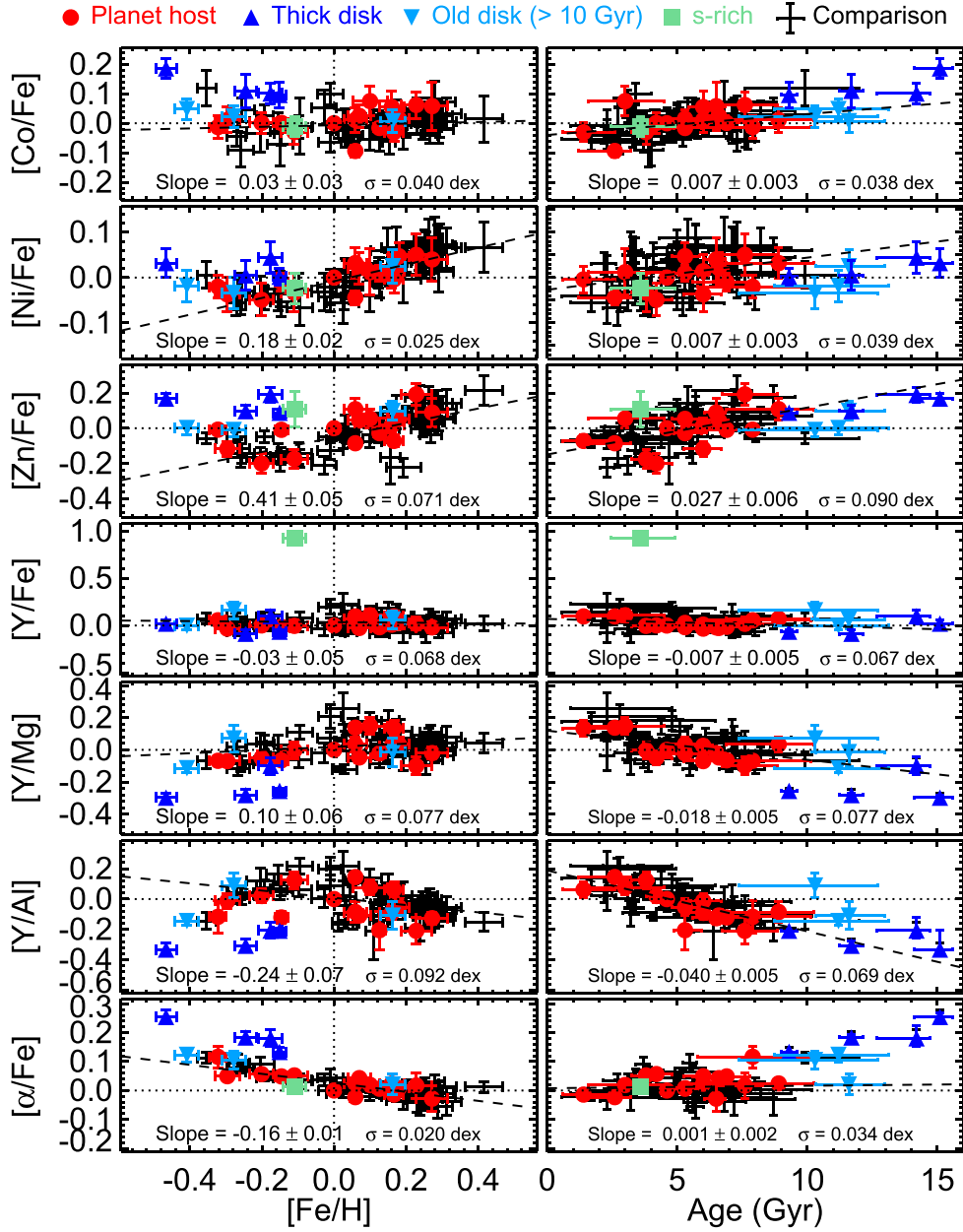
Figure 6. Same as Fig. 4, but for the final seven element ratios.

efficiently than in those planet hosts, or that those planet-hosting stars engulfed rocky material through the ingestion of rocky planets, or of giant planets that formed from a sizeable rocky core of a few Earth masses. It is important to recognize that we are implicitly assuming that the comparison stars did not form planets, which might be biased towards the current observations. As mentioned in Section 2, at the time of selection those objects were not known to host planets. However, the occurrence rates of planets in the *Kepler* field continue to be debated (Hsu et al. 2019) and could be as high as 1.0 (Borucki 2016). Results from microlensing (Cassan et al. 2012) also indicate a high probability that a given star hosts a planet. A high planetary occurrence rate greatly complicates the selection of comparison stars and therefore the identification of abundance differences between planet- and non-planet-hosting stars. We warn our readers that although the comparison stars do not

have planets detected so far, most of them probably have planets. If so, the observed abundance patterns of planet hosts would imply, instead of planet existence effects, the signatures related to the extent of the fractionation of refractory materials from volatile materials during planet formation (Wang, Lineweaver & Ireland 2019a), or to the frequency of planet engulfment events. However, a detailed discussion on such a scenario is beyond the scope of this paper.

The results in this study confirm the considerable diversity in the chemical compositions of planet-hosting stars with respect to comparison stars, i.e. a large spread of the $T_{\rm cond}$ slopes of the refractory elements. Interestingly, the total spread in the GCE corrected $T_{\rm cond}$ slopes, $\sim 2.5 \times 10^{-4}$ dex K^{-1}, is about the same in our sample and in Bedell et al. (2018). Assuming a range of 800 K for $T_{\rm cond}$ of the refractories, this might indicate that the

Table 3. Results of the linear fitting of [X/Fe] versus [Fe/H] for the comparison stars excluding thick disc objects and stars with ages $\geq$10 Gyr. The coefficients are [X/Fe] = $a \times$ [Fe/H] + b.

Name	a (dex^{-1})	b (dex)
[C/Fe]	-0.118 ± 0.055	0.023 ± 0.011
[O/Fe]	-0.200 ± 0.023	-0.010 ± 0.004
[Na/Fe]	0.188 ± 0.045	0.032 ± 0.009
[Mg/Fe]	-0.125 ± 0.025	0.014 ± 0.005
[Al/Fe]	0.214 ± 0.053	0.025 ± 0.011
[Si/Fe]	-0.001 ± 0.019	0.031 ± 0.004
[S/Fe]	-0.103 ± 0.048	0.042 ± 0.009
[Ca/Fe]	-0.163 ± 0.011	0.022 ± 0.002
[Sc/Fe]	0.411 ± 0.044	-0.025 ± 0.009
[Ti I/Fe]	-0.101 ± 0.020	0.035 ± 0.004
[Ti II/Fe]	-0.113 ± 0.025	0.058 ± 0.005
[V/Fe]	-0.207 ± 0.037	0.018 ± 0.007
[Cr/Fe]	0.072 ± 0.017	0.006 ± 0.003
[Mn/Fe]	-0.131 ± 0.029	-0.012 ± 0.006
[Co/Fe]	0.027 ± 0.029	-0.007 ± 0.006
[Ni/Fe]	0.184 ± 0.018	-0.008 ± 0.004
[Zn/Fe]	0.411 ± 0.052	-0.052 ± 0.010
[Y/Fe]	-0.028 ± 0.050	0.035 ± 0.010

Table 4. Results of the linear fitting of [X/Fe] versus ages for the comparison stars excluding thick disc objects and stars with ages $\geq$10 Gyr. The coefficients are [X/Fe] = $a \times$ age + b.

Name	a (Gyr^{-1})	b (dex)
[C/Fe]	0.013 ± 0.005	-0.053 ± 0.028
[O/Fe]	0.002 ± 0.003	-0.039 ± 0.018
[Na/Fe]	0.001 ± 0.005	0.045 ± 0.026
[Mg/Fe]	0.011 ± 0.003	-0.054 ± 0.013
[Al/Fe]	0.033 ± 0.004	-0.123 ± 0.021
[Si/Fe]	-0.000 ± 0.002	0.032 ± 0.010
[S/Fe]	0.003 ± 0.005	0.020 ± 0.026
[Ca/Fe]	-0.002 ± 0.002	0.019 ± 0.013
[Sc/Fe]	0.024 ± 0.006	-0.107 ± 0.032
[Ti I/Fe]	0.007 ± 0.002	-0.009 ± 0.011
[Ti II/Fe]	0.007 ± 0.003	0.012 ± 0.014
[V/Fe]	-0.013 ± 0.004	0.064 ± 0.022
[Cr/Fe]	0.001 ± 0.002	0.005 ± 0.010
[Mn/Fe]	-0.012 ± 0.003	0.038 ± 0.015
[Co/Fe]	0.007 ± 0.003	-0.040 ± 0.014
[Ni/Fe]	0.007 ± 0.003	-0.027 ± 0.015
[Zn/Fe]	0.027 ± 0.006	-0.149 ± 0.034
[Y/Fe]	-0.007 ± 0.005	0.069 ± 0.025

'planet-induced effect' has a maximum amplitude of 0.2 dex. This is exactly what has been observed in the most extreme cases of abundance difference in binary pairs: Ramírez et al. (2019) and Nagar et al. (2020) found a difference between the binary components HIP 34407/HIP 34426 of 0.2 dex in the refractory elements, and Oh et al. (2018) also found a difference of 0.2 dex in refractory elements for the binary HD 240430/HD 240429. There are a variety of possibilities to explain such chemical diversity that we consider below.

In the context of the M09 hypothesis, the various aspects that can influence the composition of the planet-hosting star include the following. (1) The chemical composition of the accreted material: the degree of the change in the composition of the host star will increase with the difference in the composition between the
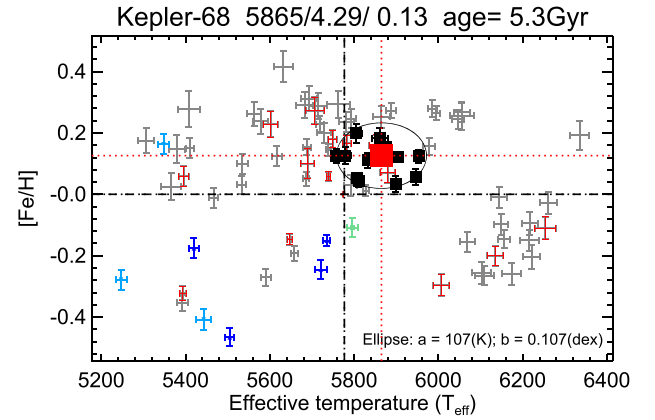

Figure 7. [Fe/H] versus effective temperature ($T_{\rm eff}$). For the planet host Kepler-68 (large red square), the 12 nearest comparison stars are shown as black squares along with their maximum distance in $T_{\rm eff}$ and [Fe/H]. An identical approach is applied to obtain the nearest comparison stars for all planet hosts. The colours are as in Fig. 4.

accreted material and the host star. The formation of terrestrial planets, and their numbers, masses (or more explicitly, densities) may induce changes in the planet host's chemical composition. (2) The amount of accreted material: the extent to which the host star's chemical composition changes will depend on the amount of material that is accreted (assuming it is of a different chemical composition). This quantity may be affected, again, by the number of planets formed and their masses/densities. (3) The simulation results by Bitsch et al. (2018) predicted that different formation locations of planets (inside/outside e.g. H_2O or CO ice line) may play an important role in changing the surface abundance ratios of their host stars for e.g. [Fe/O] or [Fe/C]. (4) The time-scale for accretion: during the protostellar evolution, the size of the convective envelope decreases such that for a fixed amount of accreted material, a larger convection zone will dilute the accreted material and minimize any potential change in the stellar surface composition. In addition, cooler stars have deeper convection zones, therefore, the polluting material should be more diluted in the photosphere of the star. However, we do not find any clear relation between $T_{\rm cond}$ slopes and $T_{\rm eff}$ in our study. The lack of correlation between $T_{\rm cond}$ slopes and $T_{\rm eff}$ is also reported in Ramírez et al. (2014).

Furthermore, recently the M09 signature has been related to the formation of distant giant planets (Booth & Owen 2020), as those planets could trap significant amounts of dust exterior to their orbits, preventing the dust from being accreted into the star, thus explaining the lower abundance of refractories in the Sun.

Another potential scenario, namely planet engulfment scenario, was proposed initially by Pinsonneault et al. (2001) to explain the differences in elemental abundances in stars with and without planets. In this scenario, the chemical compositions of the planet-hosting star might be enhanced in refractory elements because of the post-formation accretion of inner planets/material. This scenario is based on the assumption that the presence of a close-in gaseous planet might scatter or otherwise perturb the inner planets on to the surface of their host star, thus adding a large amount of H-depleted material, enhancing the stellar photospheric abundances for refractories. This has been reported and discussed in several spectroscopic studies of wide binaries by e.g. Oh et al. (2018), Liu et al. (2018), Ramírez et al. (2019), and Nagar et al. (2020), where a planet-hosting component in a binary system could be
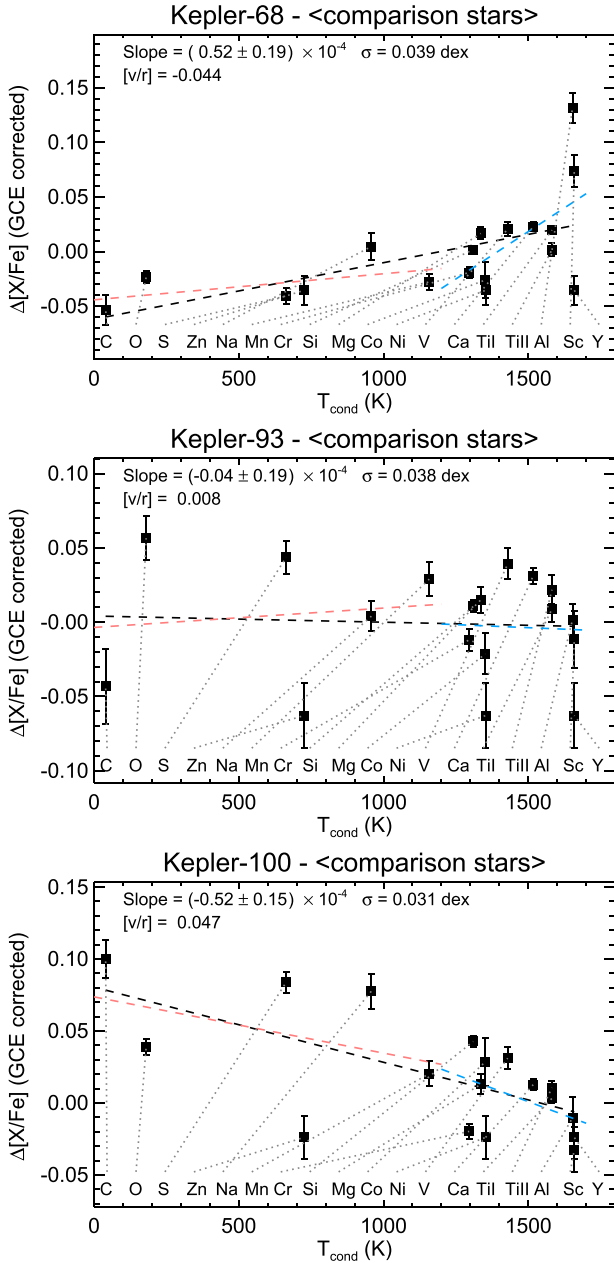
Figure 8. Abundance differences between the planet hosts Kepler-68 (upper), Kepler-93 (middle), and Kepler-100 (lower) and the average of the comparison stars (Δ[X/Fe], with GCE corrections applied) versus condensation temperature ($T_{\rm cond}$). The error bars represent the total uncertainties as described in the text. The slope, uncertainty, and dispersion about the linear fit are shown for all elements (dashed black line). The ratio of volatile (vol; $T_{\rm cond} < 1200$K) to refractory (ref; $T_{\rm cond} > 1200$K) elements, [v/r], is also written. The dashed pink and blue lines are the linear fits to the volatile and refractory elements, respectively.

enriched in refractories, when compared to another component in this system. Similar phenomena have been found in open clusters, where the peculiar star in on open cluster is more metal rich than the average of the cluster stars (e.g. Spina et al. 2015). In addition to the planet formation scenario proposed by M09, the planet engulfment scenario can also explain the mixed observed $T_{\rm cond}$ trends in our study. For example, stellar–planetary systems

with close-in Neptunes or Jupiters should have experienced strong dynamical interactions in the past, thus it is possible that they have induced more material to fall into the star. It is possible that those planet hosts showing positive $T_{\rm cond}$ trends have engulfed more material from their planetary systems depending on the architecture of the system.

Finally, there are alternative possibilities to explain the diversity in the chemical compositions of planet-hosting stars that do not involve planets (e.g. Önehag et al. 2011). Inhomogeneous chemical evolution would produce element-to-element differences amongst stars. In that scenario, one might expect to see chemical abundance differences possibly attributed to different nucleosynthetic processes. While we have attempted to correct for GCE, our sample is small and the corrections applied may not be sufficiently accurate to reveal subtle abundance trends amongst our sample. In addition, the $T_{\rm cond}$ of Lodders (2003) is calculated based on the solar elemental abundances at a fixed solar nebular pressure. However, studies have shown that the sequence of condensation and thus the composition of condensed materials would vary depending on the nebular pressures and the stellar elemental abundances (Ebel & Grossman 2000; Unterborn & Panero 2017). This may further complicate the exploration of planet signatures based on the abundance versus $T_{\rm cond}$ trends.

5 CONCLUSIONS

We present a differential analysis of 16 planet-hosting stars and 68 comparison objects using high-resolution, high S/N spectra. We obtained high-precision stellar parameters and relative chemical abundance ratios. Average uncertainties for $T_{\rm eff}$, $\log g$, and [Fe/H] are 15 K, 0.034 cm s^{-2}, and 0.012 dex, respectively. The average uncertainties for abundance ratios [X/H] range from 0.010 dex (Si) to 0.042 dex (C). The abundance ratios are corrected for GCE using the trends between [X/Fe] versus ages. For each planet host, we identify the nearest comparison stars in terms of effective temperature and metallicity. We then examine the abundance differences between the planet host and the average of the comparison stars as a function of dust condensation temperature. We confirm that the Sun is chemically different from its comparison stars; the trend between abundance differences and $T_{\rm cond}$ is negative. While about half of the planet hosts exhibit similar negative $T_{\rm cond}$–abundance trends, the other half, however, exhibit positive $T_{\rm cond}$–abundance trends.

It remains unclear why there is such chemical diversity among the planet-hosting stars with respect to the comparison stars. The range of $T_{\rm cond}$ slopes observed might reflect the range of possible planet-induced effects present in the planet-hosting stars, from the sequestration of rocky material (refractory poor) to the possible ingestion of planets (refractory rich). In the context of the M09 work and potential chemical signatures of planet formation, the time-scale, location, efficiency, and degree of planet formation could all affect stellar chemical compositions. Indeed, there are considerable challenges in finding an appropriate comparison sample for each of the planet hosts. Alternatively, planet engulfment, inhomogeneous chemical evolution, or inconsistent condensation processes amongst different stars could also explain such differences.

Finally, following Wang et al. (2019b), in a future paper (Wang et al., in preparation), we will use the high-precision chemical abundances of planet hosts from this paper to infer the bulk composition and internal structure of exoplanets.

Table 5. Results of the linear fitting of [X/Fe] versus T_{cond} for each planet host. The coefficients are $[X/Fe] = a \times T_{cond} + b$.

Name	a (all) $(10^{-4} \text{ K dex}^{-1})$	b (all) (dex)	a (vol) $(10^{-4} \text{ K dex}^{-1})$	b (vol) (dex)	a (ref) $(10^{-4} \text{ K dex}^{-1})$	b (ref) (dex)	...
Sun (Iris)	-0.317 ± 0.119	0.038 ± 0.015	-0.473 ± 0.248	0.044 ± 0.018	-0.597 ± 0.526	0.038 ± 0.015	...
HD 1461	-0.245 ± 0.098	0.040 ± 0.013	-0.200 ± 0.364	0.040 ± 0.027	0.082 ± 0.203	0.040 ± 0.013	...
EPIC 220709978	-0.249 ± 0.105	0.020 ± 0.013	-0.080 ± 0.376	0.011 ± 0.028	-0.545 ± 0.245	0.020 ± 0.013	...
EPIC 212357477	-0.541 ± 0.248	0.096 ± 0.032	-1.254 ± 0.491	0.128 ± 0.036	-0.282 ± 1.036	0.096 ± 0.032	...
Kepler-37	0.365 ± 0.189	-0.047 ± 0.025	0.483 ± 0.496	-0.053 ± 0.037	0.083 ± 0.751	-0.047 ± 0.025	...
Kepler-408	0.320 ± 0.155	-0.048 ± 0.020	-0.407 ± 0.276	-0.013 ± 0.020	1.060 ± 0.498	-0.048 ± 0.020	...
Kepler-21	-0.167 ± 0.180	0.011 ± 0.023	-0.451 ± 0.673	0.023 ± 0.050	-0.321 ± 0.360	0.011 ± 0.023	...
HD 179079	-0.172 ± 0.147	0.023 ± 0.019	-0.428 ± 0.495	0.035 ± 0.037	0.151 ± 0.439	0.023 ± 0.019	...
Kepler-131	0.335 ± 0.221	-0.035 ± 0.028	-0.548 ± 0.452	0.010 ± 0.033	1.592 ± 0.723	-0.035 ± 0.028	...
Kepler-68	0.518 ± 0.191	-0.062 ± 0.025	0.239 ± 0.191	-0.044 ± 0.014	1.736 ± 0.885	-0.062 ± 0.025	...
Kepler-93	-0.042 ± 0.190	0.004 ± 0.024	0.130 ± 0.551	-0.004 ± 0.041	-0.082 ± 0.711	0.004 ± 0.024	...
Kepler-100	-0.522 ± 0.151	0.080 ± 0.019	-0.391 ± 0.499	0.074 ± 0.037	-0.750 ± 0.477	0.080 ± 0.019	...
Kepler-409	-0.248 ± 0.193	0.027 ± 0.025	0.372 ± 0.535	-0.008 ± 0.043	-0.757 ± 0.542	0.027 ± 0.025	...
Kepler-96	0.155 ± 0.225	-0.029 ± 0.029	-0.531 ± 0.552	0.003 ± 0.041	0.726 ± 0.818	-0.029 ± 0.029	...
HD 190360	-0.149 ± 0.210	0.053 ± 0.028	-0.945 ± 0.374	0.084 ± 0.028	-0.170 ± 0.747	0.053 ± 0.028	...
HD 219828	-0.160 ± 0.115	0.029 ± 0.015	0.004 ± 0.300	0.026 ± 0.022	0.666 ± 0.362	0.029 ± 0.015	...

Note. This table is published in its entirety in the electronic edition of the paper. A portion is shown here for guidance regarding its content.
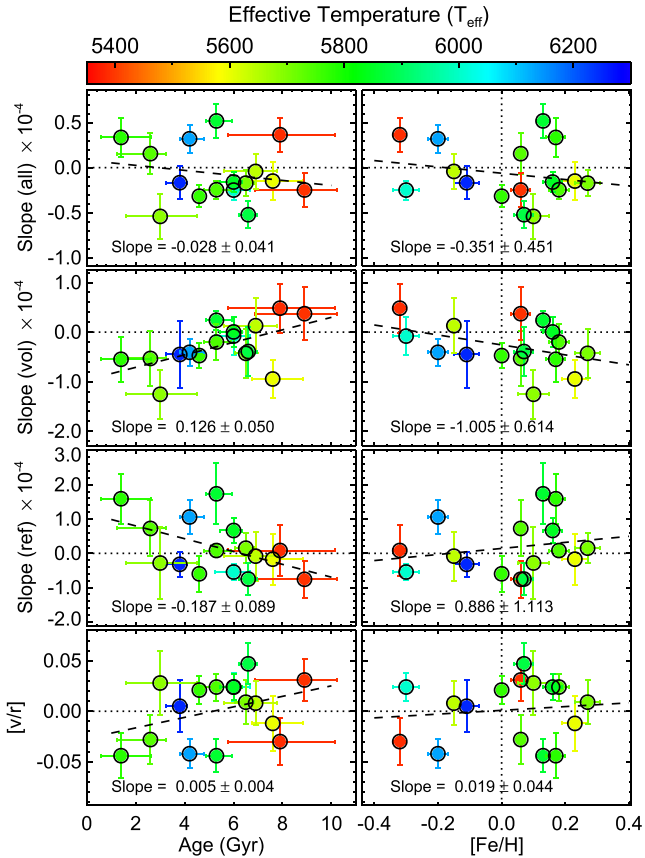
Figure 9. Summary of the slope of $\Delta[X/Fe]$, GCE corrections applied versus T_{cond} for the planet hosts versus age (left-hand panels) and [Fe/H] (right-hand panels). The top panels include the slope of $\Delta[X/Fe]$ for all elements. The second top panels include the slope of $\Delta[X/Fe]$ for the volatile elements ($T_{cond} < 1200$ K). The second bottom panels include the slope of $\Delta[X/Fe]$ for the refractory elements ($T_{cond} > 1200$ K). The bottom panels show the average $\Delta[X/Fe]$ for the volatile elements minus the average $\Delta[X/Fe]$ for the refractory elements. The data are colour coded by the effective temperature.

REFERENCES

Acuña L., 2019, MSc thesis, Lund University, Skåne, Sweden

Adibekyan V. Z., González Hernández J. I., Delgado Mena E., Sousa S. G., Santos N. C., Israelian G., Figueira P., Bertran de Lis S., 2014, A&A, 564, L15

Bailer-Jones C. A. L., Rybizki J., Fouesneau M., Mantelet G., Andrae R., 2018, AJ, 156, 58

Bedell M., Meléndez J., Bean J. L., Ramírez I., Leite P., Asplund M., 2014, ApJ, 795, 23

Bedell M. et al., 2018, ApJ, 865, 68

Bensby T., Feltzing S., Oey M. S., 2014, A&A, 562, A71

Bitsch B., Forsberg R., Liu F., Johansen A., 2018, MNRAS, 479, 3690

Booth R. A., Owen J. E., 2020, MNRAS, 493, 5079

Borucki W. J., 2016, Rep. Progress Phys., 79, 036901

Boss A. P., 1997, Science, 276, 1836

Brewer J. M., Fischer D. A., Valenti J. A., Piskunov N., 2016, ApJS, 225, 32

Cassan A. et al., 2012, Nature, 481, 167

Demarque P., Woo J. H., Kim Y. C., Yi S. K., 2004, ApJS, 155, 667

Ebel D. S., Grossman L., 2000, Geochim. Cosmochim. Acta, 64, 339

Epstein C. R., Johnson J. A., Dong S., Udalski A., Gould A., Becker G., 2010, ApJ, 709, 447

Fischer D. A., Valenti J., 2005, ApJ, 622, 1102

Gaia Collaboration et al., 2016, A&A, 595, A1

Gaia Collaboration et al., 2018, A&A, 616, A1

Gonzalez G., 1997, MNRAS, 285, 403

Gonzalez G., Carlson M. K., Tobin R. W., 2010, MNRAS, 407, 314

González Hernández J. I., Israelian G., Santos N. C., Sousa S., Delgado-Mena E., Neves V., Udry S., 2010, ApJ, 720, 1592

González Hernández J. I., Delgado-Mena E., Sousa S. G., Israelian G., Santos N. C., Adibekyan V. Z., Udry S., 2013, A&A, 552, A6

Gustafsson B., 2018a, A&A, 616, A91

Gustafsson B., 2018b, A&A, 620, A53

Han E., Wang S. X., Wright J. T., Feng Y. K., Zhao M., Fakhouri O., Brown J. I., Hancock C., 2014, PASP, 126, 827

Hsu D. C., Ford E. B., Ragozzine D., Ashby K., 2019, AJ, 158, 109

Jofré P., Jackson J., Tucci Maia M., 2020, A&A, 633, L9

Lin J. et al., 2020, MNRAS, 491, 2043

Liu F., Asplund M., Ramirez I., Yong D., Melendez J., 2014, MNRAS, 442, L51

Liu F. et al., 2016, MNRAS, 456, 2636

Liu F., Yong D., Asplund M., Feltzing S., Mustill A. J., Meléndez J., Ramírez I., Lin J., 2018, A&A, 614, A138

Lodders K., 2003, ApJ, 591, 1220

Mayor M., Queloz D., 1995, Nature, 378, 355

Meléndez J., Asplund M., Gustafsson B., Yong D., 2009, ApJ, 704, L66 (M09)

Meléndez J. et al., 2012, A&A, 543, A29

Nagar T., Spina L., Karakas A. I., 2020, ApJ, 888, L9

Nissen P. E., 2015, A&A, 579, A52

Nissen P. E., 2016, A&A, 593, A65

Nissen P. E., Gustafsson B., 2018, A&AR, 26, 6

Oh S., Price-Whelan A. M., Brewer J. M., Hogg D. W., Spergel D. N., Myles J., 2018, ApJ, 854, 138

Önehag A., Korn A., Gustafsson B., Stempels E., Vandenberg D. A., 2011, A&A, 528, A85

Petigura E. A. et al., 2017, AJ, 154, 107

Pinsonneault M. H., DePoy D. L., Coffee M., 2001, ApJ, 556, L59

Pollack J. B., Hubickyj O., Bodenheimer P., Lissauer J. J., Podolak M., Greenzweig Y., 1996, Icarus, 124, 62

Ramírez I., Meléndez J., 2005, ApJ, 626, 465

Ramírez I., Allende Prieto C., Lambert D. L., 2007, A&A, 465, 271

Ramírez I., Meléndez J., Asplund M., 2009, A&A, 508, L17

Ramírez I., Asplund M., Baumann P., Meléndez J., Bensby T., 2010, A&A, 521, A33

Ramírez I. et al., 2014, A&A, 572, A48

Ramírez I., Khanal S., Lichon S. J., Chanamé J., Endl M., Meléndez J., Lambert D. L., 2019, MNRAS, 490, 2448

Reddy B. E., Tomkin J., Lambert D. L., Allende Prieto C., 2003, MNRAS, 340, 304

Schuler S. C., Flateau D., Cunha K., King J. R., Ghezzi L., Smith V. V., 2011, ApJ, 732, 55

Schuler S. C. et al., 2015, ApJ, 815, 5

Spina L. et al., 2015, A&A, 582, L6

Spina L., Meléndez J., Ramírez I., 2016, A&A, 585, A152

Spina L., Meléndez J., Casey A. R., Karakas A. I., Tucci Maia M., 2018a, ApJ, 863, 179

Spina L. et al., 2018b, MNRAS, 474, 2580

Unterborn C. T., Panerao W. R., 2017, ApJ, 845, 61

Venn K. A., Irwin M., Shetrone M. D., Tout C. A., Hill V., Tolstoy E., 2004, AJ, 128, 1177

Vogt S. S. et al., 1994, in Crawford D. L., Craine E. R., eds, Proc. SPIE Vol. 2198, Instrumentation in Astronomy VIII. SPIE, Bellingham, p. 362

Wang H. S., Lineweaver C. H., Ireland T. R., 2019a, Icarus, 328, 287

Wang H. S., Liu F., Ireland T. R., Brasser R., Yong D., Lineweaver C. H., 2019b, MNRAS, 482, 2222

Winn J. N., Fabrycky D. C., 2015, ARA&A, 53, 409

SUPPORTING INFORMATION

Supplementary data are available at *MNRAS* online.

Table 1. Stellar parameters and ages for the program stars.
Table 2. Relative abundances for the program stars.
Table 5. Results of the linear fitting of [X/Fe] versus T_{cond} for each planet host.
Table A1. The line list and equivalent width measurements adopted for our analysis.

Please note: Oxford University Press is not responsible for the content or functionality of any supporting materials supplied by the authors. Any queries (other than missing material) should be directed to the corresponding author for the article.

APPENDIX A: EXTRA FIGURE

In Fig. A1, we show the same summary as in Fig. 9 but for the comparison stars. There are subtle trends with [Fe/H], which would suggest that it is important to restrict the range in [Fe/H] for the comparison stars.
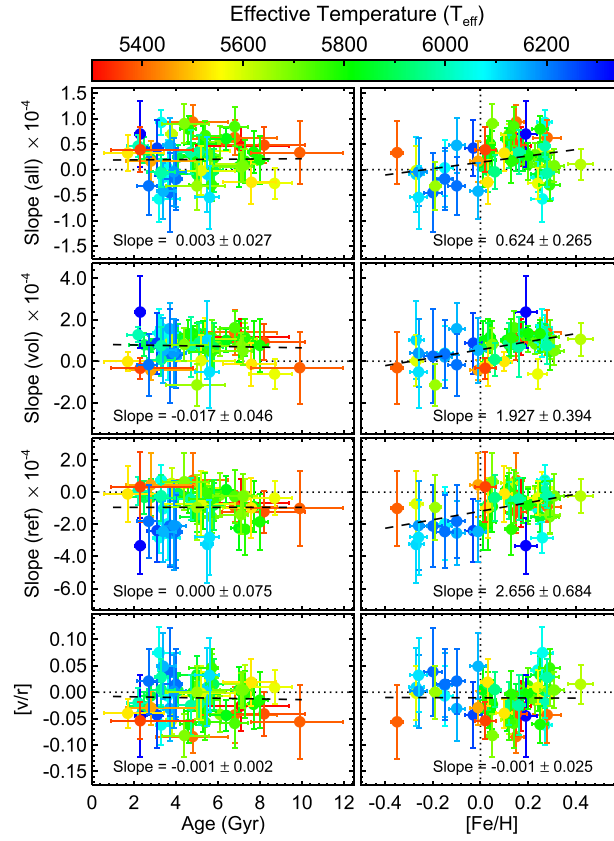
Figure A1. Same as Fig. 9, but for the comparison stars.

This paper has been typeset from a TeX/LaTeX file prepared by the author.